ACS OMEGA

Open Access

http://pubs.acs.org/journal/acsodf

Article

Electrical and Thermal Properties of Surface-Modified Copper Nanowire/Polystyrene Nanocomposites through Latex Blending

Hyeon Sik Eom, Dong Won Kim, Keon-Soo Jang,* and Seong Jae Lee*

Cite This: *ACS Omega* 2023, 8, 46955−46966

Read Online

ACCESS | Metrics & More | Article Recommendations

ABSTRACT: The incorporation of conductive nanofillers into an insulating polymer matrix commonly leads to nanocomposites with good electrical, thermal, and mechanical properties. In this study, copper nanowires (CuNWs) and polystyrene (PS) microspheres were synthesized along with the fabrication of CuNW/PS polymer nanocomposites. The electrical, thermal, mechanical, rheological, and morphological properties of the CuNW/PS nanocomposites were examined. The CuNWs were homogeneously dispersed in the PS matrix through latex blending. For the CuNW/PS nanocomposites, the storage modulus was higher than the loss modulus at all frequencies, indicating their elastic-dominant behavior. The electrical and thermal conductivities of the nanocomposites increased with an increasing CuNW content. Using a mixed dispersion of two monodisperse PS particles of 500 nm and 5 μm in diameter resulted in the highest electrical conductivity (ca. 10° S/m for 30 wt % nanofillers) among the nanocomposites. In addition, the introduction of silica- and polydopamine-coated CuNWs as nanofillers imparted insulation properties to the nanocomposites, with electrical conductivities to 10^{-10}−10^{-8} S/m. When using 500 nm PS particles, the thermal conductivity of the surface-modified CuNW/PS nanocomposite at 30 wt % of CuNW was enhanced to 0.22 W/m·K compared to 0.17 W/m·K for its unmodified counterpart. We have achieved multiple innovative approaches, including the use of mixed particle sizes, surface modification of CuNW, and the exploration of elastic-dominant behavior. This enhanced thermal conductivity, coupled with the attainment of insulation properties, presents a distinct advantage for thermal interface material (TIM) applications.

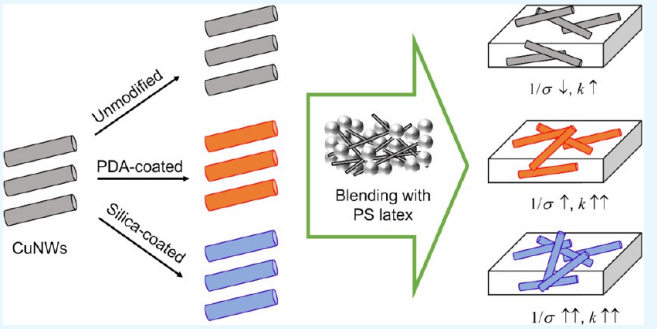

1. INTRODUCTION

Polymers and polymer nanocomposites are widely used in various fields owing to their excellent processability, lightness, low cost, and good resistance to chemicals despite their relatively low mechanical properties and thermal and electrical conductivities, compared to metals and ceramics.[1] For instance, in electrically conductive polymer nanocomposites, the low electrical conductivity of polymers is overcome by embedding highly conductive nanofillers such as carbon nanotubes (CNTs), graphene, and metal nanowires into a polymer matrix.[2−6] Nanosized fillers substantially enhance the electrical, thermal, and mechanical properties of the nanocomposites because of their large specific surface areas compared with microsized fillers at the same concentration.[7−9]

Typically, the conductivity of polymer nanocomposites is related to the size and concentration of the nanofillers. Low concentrations and aspect ratios of nanofillers cause failure to achieve electrical networks among the nanofillers, leading to electrical insulation.[10] However, electrically conductive materials can be produced above the electrical percolation threshold of nanofillers.[11] The poor dispersion of nanofillers in a polymer matrix results in agglomeration and degrades the properties of the nanocomposites, despite high filler concentrations. Therefore, the compatibilities between nanofillers and between nanofillers and the polymer matrix are important for improving the dispersion of nanofillers in the matrix.

In terms of preparation of a polymer matrix, spherical polystyrene (PS) particles can be synthesized via suspension,[12,13] dispersion,[14−16] precipitation,[17] and emulsion[18] polymerization. Dispersion polymerization yields monodisperse microparticles, whereas in suspension polymerization, 1−1000 μm particles with various sizes and monodispersity are obtained by tailoring the interfacial tension and suspension stability.[19] However, these polymerization methods have difficulty producing submicron-sized particles with sizes of <1 μm.[20] Precipitation polymerization produces more robust microparticles with a higher cross-link density but less monodispersity, compared with dispersion polymerization.[21]

Received: September 7, 2023
Revised: October 21, 2023
Accepted: November 17, 2023
Published: November 29, 2023

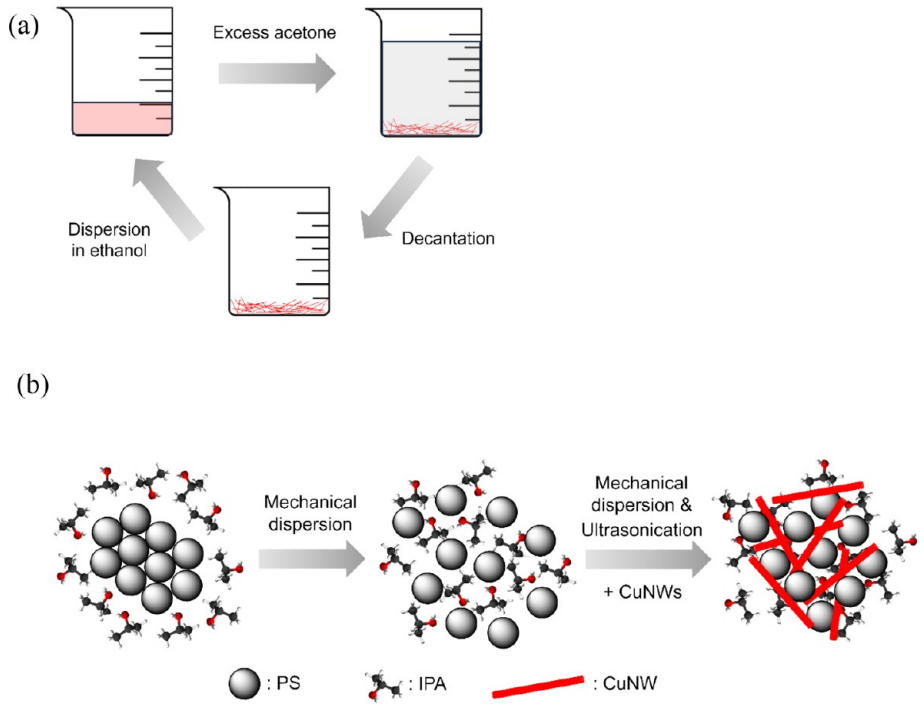

Figure 1. Schematic of the fabrication steps: (a) purification of CuNWs and (b) preparation of a homogeneous CuNW/PS/IPA mixture.

Emulsion polymerization is suitable for synthesizing monodisperse PS submicroparticles.[21] In particular, emulsifier-free emulsion polymerization using only an initiator is preferred because it does not require the removal of emulsifiers and surfactants.[22,23]

Metal nanowires exhibit higher specific aspect ratios, better optical properties, and higher thermal and electrical conductivities in comparison to electrically conductive carbon-based nanofillers (CNTs, graphene, and carbon fibers). Among the different types of metal nanowires, copper nanowires (CuNWs) are employed owing to their ease of fabrication with high aspect ratio, purity, and low cost (compared with silver nanowires).[24] CuNWs are routinely synthesized using the template method[25,26] and electrochemical deposition.[27] Recently, they have been synthesized via Cu reduction in aqueous solutions, which is known as aqueous-media reduction.[28] The specific aspect ratio and oxidation can be controlled by adjusting the capping agent, the reaction temperature, and the reaction time. For instance, a low reaction temperature and short reaction time resulted in CuNWs with a low specific aspect ratio. Common capping agents include ethylenediamine (EDA),[29] polyvinylpyrrolidone (PVP), and hexadecylamine (HDA).[30] The use of EDA led to agglomeration of the nanofillers, resulting in poor properties of nanocomposites.[31] PVP is widely used for Ag and Pd growth but is unsuitable for Cu owing to no effect on suppression of Cu oxidation.[32] In contrast, HDA is effective for growing CuNWs without oxidation; thus, HDA is widely used.

In the realm of electrical applications, the desirability of possessing robust thermal and electrical conductivities is widely acknowledged.[33−35] However, there exist scenarios where materials exhibiting electrical insulation alongside thermal conduction find utility.[36−40] Notably, such materials find application as thermally conductive electrical insulators,[36,37] facilitating thermal management in electronics,[38] enhancing sensor capabilities,[39] and enabling the development of efficient thermal barrier coatings.[40] It is important to note that the relationship between electrical and thermal conductivities is intimately intertwined. Materials boasting high thermal conductivity often concurrently demonstrate elevated electrical conductivity.[33−35] To address this interrelation, a strategic approach involves the encasing of electrically conductive materials with insulating layers, thereby enabling the curtailment of electrical conductivity while upholding thermal transfer characteristics. This intriguing interplay of high thermal conductivity with adjustable electrical conductivities thereby unveils a realm of extensive applicability across various domains. In this study, PS was selected as the matrix of polymer nanocomposites because of its good mechanical properties, thermal stability, and processability. 5 μm and 500 nm PS microspheres synthesized via dispersion polymerization and emulsifier-free emulsion polymerization, respectively, were compared. CuNWs synthesized via aqueous media reduction were chosen as conductive nanofillers. Dextrose, which is commonly used in the case of HDA-capping systems because of its high purity and monodispersity, was selected as the reductant.[30] Furthermore, CuNW surfaces were coated with silica (SiO_2) and polydopamine (PDA) to induce electrical insulation, maintaining thermal conductivity for applications in thermal interface materials (TIMs).[41−43] Finally, thermally conductive polymer nanocomposites with electrical insulation were fabricated via latex blending and characterized.

2. EXPERIMENTAL SECTION

2.1. Materials. Copper(II) chloride dihydrate (>99%), dextrose, tetraethyl orthosilicate (TEOS, >99%), tris-(hydroxymethyl)amino methane, dopamine hydrochloride, PVP (MW = 40,000 g/mol), and HDA (>90%) were purchased from Sigma-Aldrich (St. Louis, Missouri, USA). Acetone (99.5%), ethyl alcohol (99.9%), styrene monomers (99.5%), potassium persulfate (KPS, >99%), 2,2′-azobisisobutyronatrile (AIBN, 98%), isopropyl alcohol (IPA, 99.5%), and

https://doi.org/10.1021/acsomega.3c06775
ACS Omega 2023, 8, 46955−46966

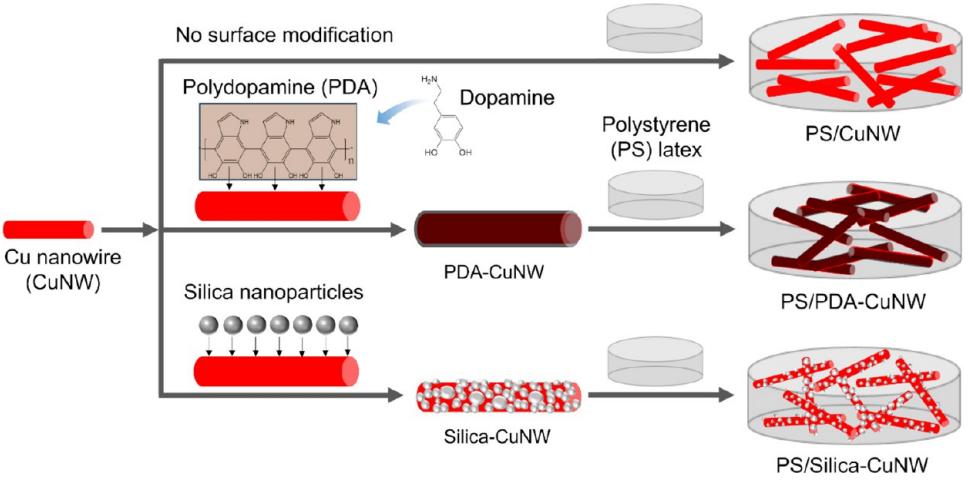

Figure 2. Overall fabrication avenues of CuNW/PS nanocomposites with and without surface modification.

1-butanol were purchased from Samchun Chemical Co. (South Korea).

2.2. Synthesis of PS Particles. *2.2.1. Synthesis of 500 nm PS Particles.* 500 nm PS monodisperse microspheres were synthesized using KPS as an initiator via emulsifier-free emulsion polymerization. First, KPS was completely dissolved in deionized (DI) water. Subsequently, ethanol, styrene, and KPS were sequentially added to a jacketed glass reactor. The resulting solution was stirred at 300 rpm for 20 min at room temperature. Then, the mixture was further stirred at 120 rpm for 24 h at 70 °C for polymerization. After polymerization, the solution was washed three times with ethanol and DI water, respectively, by a centrifuge.

2.2.2. Synthesis of 5 μm PS Particles. 5 μm PS monodisperse microspheres (5 μm) were synthesized via dispersion polymerization with an AIBN initiator. First, PVP and AIBN were dissolved in 1-butanol and styrene, respectively. These two solutions were inserted into a jacketed glass reactor and stirred at 120 rpm for 24 h at 70 °C. After polymerization, the final solution containing the PS particles was washed three times with ethanol and DI water, separately via centrifugation.

2.3. Synthesis of CuNWs. The CuNWs were synthesized by using aqueous media reduction. Dextrose as a reductant and HDA as a capping agent were sequentially dissolved in DI water. Copper chloride dihydrate was added to the solution, and the resulting solution was stirred for 12 h at room temperature to reduce the number of Cu ions in the aqueous solution. Subsequently, the CuNWs were grown in an oil bath without stirring for 10 h at 110 °C. The synthesis was terminated by quenching the mixture. The quenched mixture was then washed with acetone via centrifugation to remove the reductant and impurities such as Cu particles and short CuNWs, as shown in Figure 1a.

2.4. Surface Modification of CuNWs. *2.4.1. Silica-Coated CuNW.* The CuNW surface was coated with silica to achieve electrical insulation and high thermal conductivity for TIM applications. 0.3 g of CuNW was added to 80 mL of IPA, and the mixture was stirred at 120 rpm for 30 min at room temperature. Subsequently, 0.06 mL of TEOS was added and the final mixture was stirred at 120 rpm for 12 h at room temperature. After polymerization, the mixture was vacuum-filtered using an aspirator and then washed five times with IPA via centrifugation at 10,000 rpm for 1000 s at 4 °C.

2.4.2. PDA-Coated CuNW. The CuNW surface was also coated with PDA to achieve electrical insulation with high thermal conductivity for TIM applications. First, 1.21 g of tris(hydroxymethyl)amino methane was dissolved in 400 mL of DI water. The pH value of the aqueous solution was set to 8.5 by adding dilute hydrochloric acid. 0.1 g of CuNW was added to the aqueous solution at pH 8.5, followed by stirring at 120 rpm for 2 h. Afterward, 0.05 g of dopamine hydrochloride was added to the mixture. The CuNW surfaces were coated with PDA at different reaction times. The resulting solution was vacuum-filtered using an aspirator and then washed three times with DI water and IPA for 1000 s at 4 °C and 10,000 rpm through a centrifuge, respectively.

2.5. Preparation of the PS/CuNW Nanocomposite. *2.5.1. Dispersion of PS Particles and CuNWs.* IPA was used as a dispersion solvent because it is suitable for both hydrophobic PS microspheres and HDA-capped CuNW dispersions. 10 phr of PS was dispersed in IPA, and the suspension was stirred at 500 rpm for 1 h at room temperature. Afterward, the CuNWs were added to the suspension and dispersed by continuously stirring the entire mixture at 500 rpm for 2 h. Subsequently, the CuNW/PS/IPA mixture was further dispersed via ultrasonication at 10 W for 1 h, as shown in Figure 1b.

2.5.2. Fabrication of the PS/CuNW Nanocomposite. After a homogeneous dispersion of CuNW in the PS/IPA suspension was obtained, the whole mixture was dried at 60 °C in a vacuum oven to eliminate IPA. The dried CuNW/PS mixture was finely ground. Then, the finely ground powder was put into a mold with a diameter of 10 mm and thickness of 1 mm at 210 °C. The molten composite was held at 210 °C until the voids were removed and then pressed at 210 °C for 10 min under 10 MPa of pressure, producing a round disk-like specimen with a diameter of 10 or 25 mm and a thickness of 1 mm. The process from grinding to compression was repeated three times to completely remove the voids. Figure 2 shows the summary of fabrication routes for CuNW/PS nanocomposites with and without surface modification.

2.6. Characterization. Field-emission scanning electron microscopy (FE-SEM; Apreo, FEI, Hillsboro, Oregon, USA) was utilized to examine the morphologies of the PS particles, CuNWs, CuNW/PS powder, and fractured surface. The electron beam voltage was set to 10 kV. The specimens were sputter-coated with Au prior to the SEM observations. The dispersity of the CuNWs in the matrix was analyzed using SEM

https://doi.org/10.1021/acsomega.3c06775
ACS Omega 2023, 8, 46955−46966

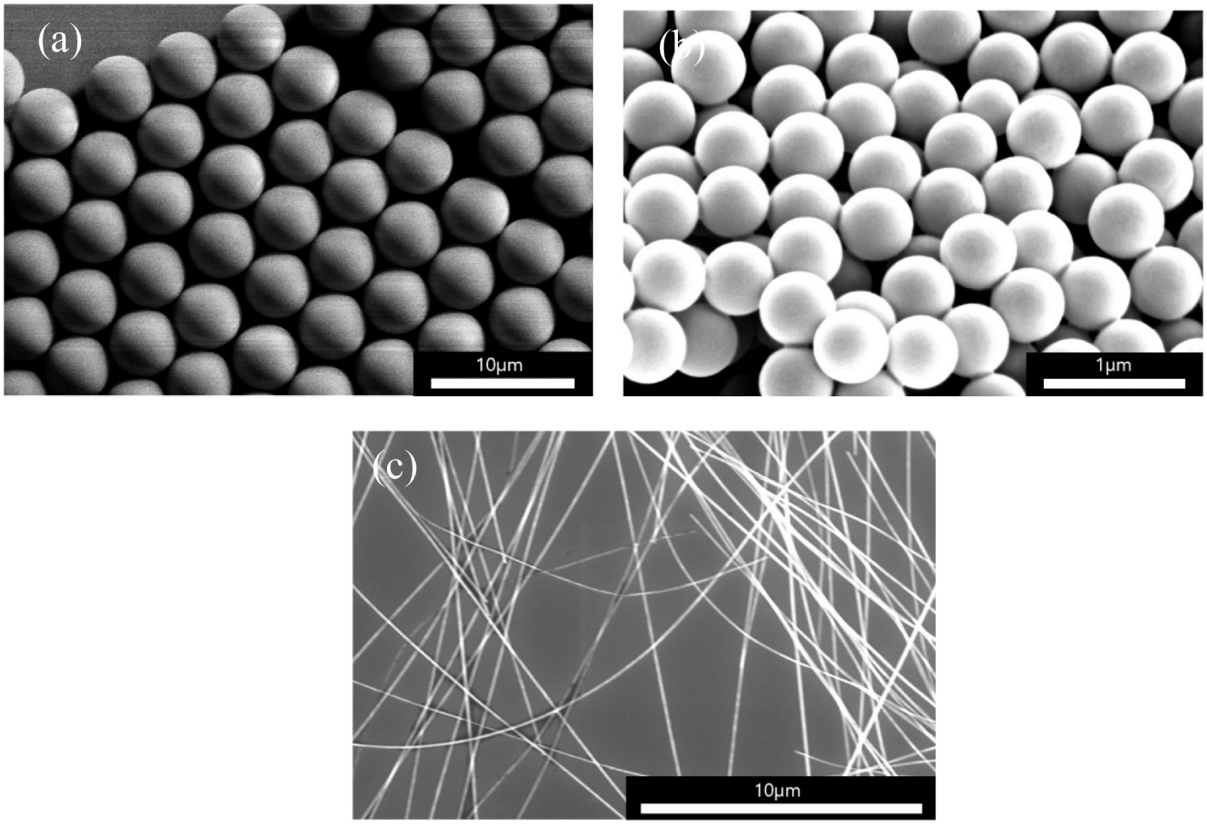

Figure 3. SEM images of (a) 5 μm (dispersion polymerization) and (b) 500 nm (emulsifier-free emulsion polymerization) PS microspheres and (c) CuNWs synthesized via aqueous media reduction.

and energy-dispersive X-ray spectroscopy (EDX) at a dwell time of 1000 μs and ×5000 magnification, with four scans.

X-ray diffraction spectroscopy (XRD; ARL EQUINOX 3000, Thermo Fisher Scientific, Waltham, Massachusetts, USA) was utilized to analyze the oxidation of Cu and silica coating on the surfaces of CuNW and silica-coated CuNW. The X-ray angle was set at 6°, with a voltage of 40 kV and a current of 30 mA.

A rotational rheometer equipped with parallel plate geometry (MCR300, Anton Paar, Graz, Austria) was used in small-amplitude oscillatory shear mode at 210 °C and a strain amplitude of 3%. Specimens were prepared by compression molding in the form of circular disks with a diameter of 25 mm and a thickness of 1 mm. A frequency sweep was performed from 0.01 to 100 rad/s to evaluate the rheological properties, such as the storage modulus and complex viscosity, of the CuNW/PS composites.

The electrical properties of the CuNW/PS composites were investigated using a picoammeter (Keithley 6487, Keithley Instruments, Solon, Ohio, USA) and a digital multimeter (Fluke 189, Fluke, Everett, Washington, USA) for sample resistances of >500 and <500 MΩ, respectively. The round disk-like specimens were 10 mm in diameter and 1 mm thick. The electrical conductivities of the nanocomposites were determined based on the following equation:

$$\sigma = \frac{d}{RS} \tag{1}$$

where σ, R, S, and d represent the electrical conductivity, resistance, cross-sectional area, and thickness of the sample, respectively.

For the measurements of thermal conductivities of the CuNW/PS nanocomposites, the z-axis thermal diffusivities were measured at room temperature (25 °C) by using a thermal conductivity measurement instrument (LFA 467 HyperFlash, NETZSCH Co., Germany). The dimensions of round disk-like specimens were a diameter of 10 mm and a thickness of 1 mm. The specific heat of the nanocomposites at room temperature (25 °C) was measured by using differential scanning calorimetry (DSC, Jade DSC Lab System, PerkinElmer Co., Waltham, Massachusetts, USA). Each sample (approximately 3 mg) was sealed between a hermetic Al pan and lid. The sample was heated at a scanning rate of 10 °C/min under a N_2 atmosphere. The thermal conductivities of the nanocomposites were finally determined from the measured values (thermal diffusivity and specific heat), based on eq 2.

$$k = \rho C_p \alpha \tag{2}$$

where k, ρ, C_p, and α represent the thermal conductivity, density, specific heat, and thermal diffusivity, respectively.

3. RESULTS AND DISCUSSION

3.1. Morphologies of PS Microspheres and CuNWs.

3.1.1. Morphologies of 500 nm and 5 μm Monodisperse PS Particles. Emulsifier-free emulsion polymerization and dispersion polymerization were utilized to synthesize 500 nm and 5 μm monodisperse PS microspheres, respectively. The monodispersity of PS can be affected by various factors such as the concentration of materials, reaction temperature, and reaction time. Thus, after the synthesis of the PS particles, their morphologies were observed by using FE-SEM. Figure 3a and b shows highly monodisperse PS microspheres. Unlike 5 μm

https://doi.org/10.1021/acsomega.3c06775
ACS Omega 2023, 8, 46955−46966

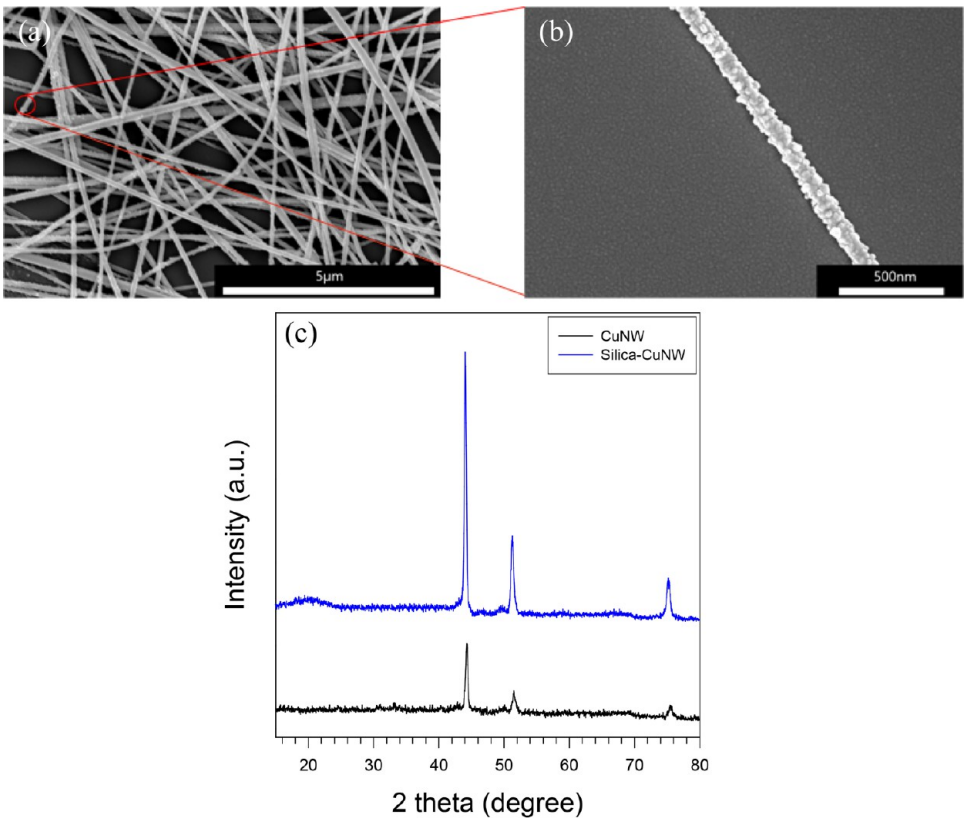

Figure 4. SEM images (a, b) of silica-coated CuNWs: (a) magnification of 20,000×, (b) magnification of 100,000×, and (c) XRD patterns of CuNWs and silica-coated CuNWs.

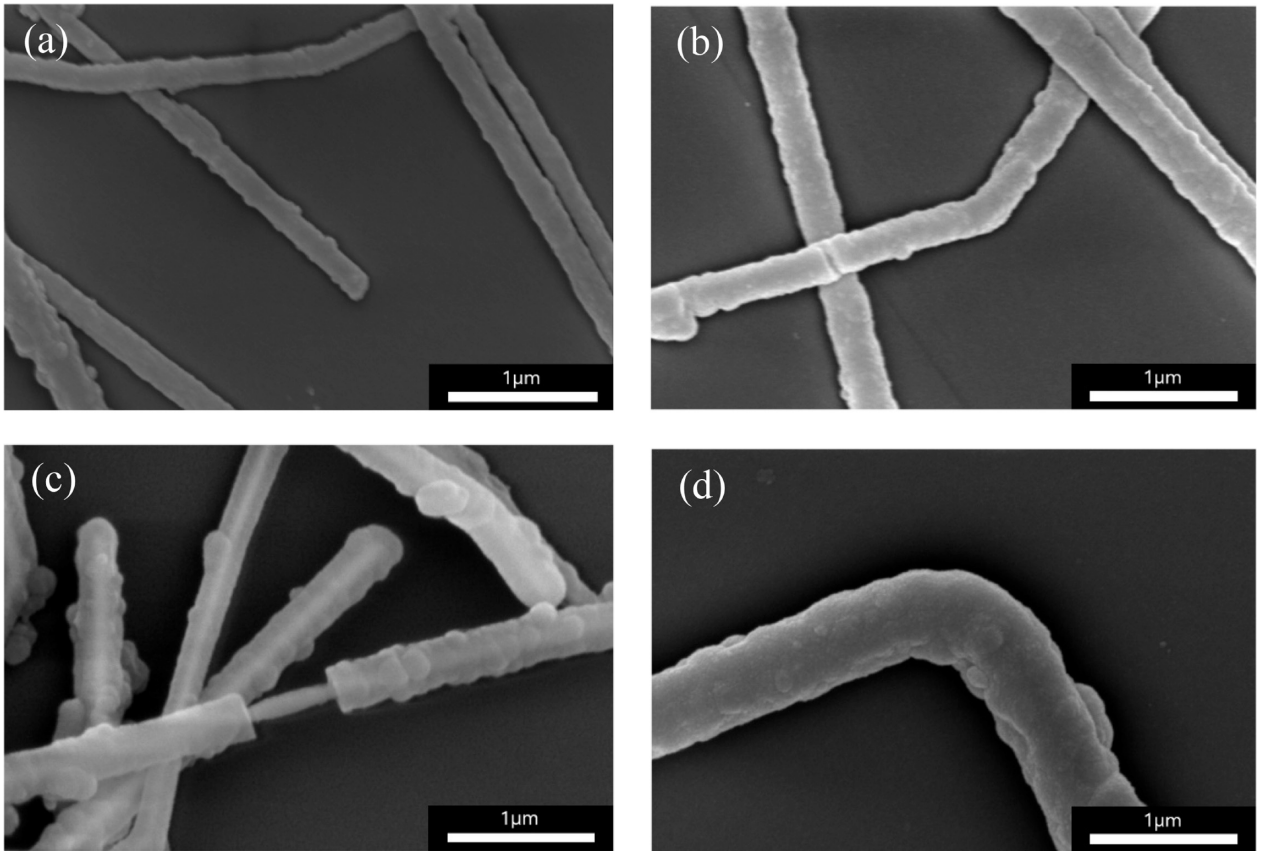

Figure 5. SEM images of PDA-coated CuNWs prepared with different reaction times: (a) 3, (b) 6, (c) 12, and (d) 24 h.

https://doi.org/10.1021/acsomega.3c06775
ACS Omega 2023, 8, 46955−46966

PS particles using a stabilizer (PVP), in the emulsifier-free synthesis of 500 nm PS particles, sulfate ions (SO_4^{2-}) generated by the decomposition of KPS are attached to the styrene monomer and the repulsive force between these sulfate ions stabilizes the latex particles and acts as a stabilizer.

3.1.2. Morphology of CuNWs. FE-SEM was performed to examine the 1D-nanostructured CuNWs grown via aqueous media reduction with HDA as a capping agent and dextrose as a reducing agent. Impurities such as Cu particles, unreacted materials, and residual reducing agents must be removed in the case of inappropriate concentrations of substances and side reactions in aqueous media reduction, as previously shown in Figure 1a. In addition, the aspect ratio of CuNW was influenced by the reaction temperature and time. Therefore, the morphologies of CuNWs were investigated to verify their uniform diameters and length. The average diameter and length of the CuNWs were 99.2 ± 21.1 nm and 54.8 ± 28.0 μm, respectively, resulting in an aspect ratio of approximately 550, as shown in Figure 3c.

3.2. Morphologies of CuNWs with Surface Modification. *3.2.1. Morphology of Silica-Coated CuNWs.* Nanofillers such as alumina (Al_2O_3), aluminum nitride (AlN), and boron nitride (BN) are routinely used as TIMs in conductive polymer nanocomposites.[44] However, a high loading of these nanofillers is required to achieve the desired thermal conductivity for TIMs. In addition, high loading generally results in the aggregation of nanofillers and heterogeneous dispersion, thereby degrading various properties. To address this issue, in this study, the surfaces of CuNWs were coated with silica (SiO_2), which provided good dispersion and electrical insulation, maintaining a high thermal conductivity. The silica-coated CuNW (SiO_2−CuNW) had an average diameter of 141.2 ± 31.7 nm and a length of 48.8 ± 29.4 μm. Their aspect ratio was slightly reduced to 345 owing to the thickness of the silica coating. Figure 4a and b shows the silica coating on the surfaces of CuNWs.

XRD spectroscopy was performed to confirm the presence of the silica coating and oxidation on the surfaces of CuNWs (Figure 4c). The XRD patterns of the CuNWs and SiO_2−CuNWs exhibited distinct peaks at 2θ = 44.7, 51.5, and 75.8°, corresponding to the (111), (200), and (220) Cu crystallographic planes, respectively. The absence of peaks ascribed to CuO confirmed the occurrence of a rare oxidation. An additional broad and weak peak at 2θ = 20.5° was observed for the SiO_2−CuNWs, which corresponded to the amorphous SiO_2 layer on the surface of CuNWs, confirming the presence of silica coating on the CuNW surface.

3.2.2. Morphology of PDA-Coated CuNWs. Similar to the SiO_2 coating, the CuNWs were coated with dopamine to maintain their thermal conductivity while adding insulation. Dopamine undergoes self-cross-linking to form PDA under weak alkaline conditions, such as pH 8.5, and exhibits strong adhesion to various substances, including metals.[45] The thickness of the PDA coating on the CuNWs was affected by the concentration of the substances and the reaction time for the PDA coating process. Thus, the aspect ratio of the PDA-coated CuNWs was examined as a function of the reaction time at the same concentration. The thickness of the PDA coating on the CuNW surfaces increased with increasing reaction time, as shown in Figure 5. The aspect ratios of the PDA-coated CuNWs decreased to 224, 200, 175, and 101, based on SEM images for reaction times of 3, 6, 12, and 24 h, respectively. The average diameter and length of PDA-coated CuNWs with different reaction times are displayed in Table 1. In this study, the optimal reaction time for the PDA coating

Table 1. Length, Diameter, and Aspect Ratio of PDA-Coated CuNW with Different Reaction Times

reaction time (h)	length (μm)	diameter (nm)	aspect ratio
0	54.8 ± 28	99.2 ± 21.1	552
3	49.3 ± 21.1	220.6 ± 33.4	224
6	54.5 ± 12.9	273 ± 30.7	200
12	52.6 ± 12.1	301.1 ± 20.1	175
24	53.6 ± 18.2	531.1 ± 19.8	101

was determined to be 3 h, as thick encapsulating PDA layers were easily damaged beyond 3 h, which yielded PDA-coated CuNWs with an average diameter of 220.6 ± 33.4 nm and a length of 49.3 ± 21.1 μm, corresponding to an aspect ratio of approximately 224.

3.3. Dispersibility of PS Microspheres and CuNWs. *3.3.1. Dispersion of CuNW/PS in IPA.* Uniform dispersion of conductive nanofillers in a polymer matrix is crucial for optimizing the properties of the nanocomposites. Proper selection of a solvent results in a uniform dispersion of the nanofillers within a polymer matrix. In this study, an amphiphilic solvent, IPA, was utilized to simultaneously disperse both PS particles and HDA-capped CuNWs. The dispersion stability of CuNWs in IPA was analyzed as a function of time after applying physical forces, such as mechanical and ultrasonic forces, as shown in Figure 6. The

Figure 6. Dispersion stability of IPA/CuNW mixtures over time after mechanical and ultrasonic dispersion.

CuNW aggregation caused by van der Waals forces was separated using physical forces, leading to the stable dispersion of CuNWs in IPA for up to 12 h without the use of additional dispersants.

3.3.2. Morphologies of CuNW/PS Nanocomposites. The dispersion of CuNWs in CuNW/PS before and after the compounding process (thermal compression) was investigated by FE-SEM, as shown in Figures 7 and 8, respectively. Figure 7 shows the morphologies of CuNW/PS mixtures with different nanofiller loadings and PS particle sizes in the powder state. The CuNW nanofillers were uniformly dispersed within the PS matrix, regardless of the PS particle size or CuNW concentration. In the case of mixed PS particles with different sizes, 500 nm PS microspheres covered the surfaces of 5 μm PS microspheres and filled the gaps between 5 μm PS particles. The fractured surfaces of CuNW/PS nanocomposites with different nanofiller loadings and PS particle sizes are shown in Figure 8. The pristine PS without the nanofillers exhibited clean fractured surfaces; however, with an increase in the nanofiller concentration, the nanocomposites increasingly exhibited traces of CuNWs, such as pulled-out marks and embedded and broken CuNWs in the matrix. In addition, the dispersion of CuNWs was visually confirmed by EDX mapping

https://doi.org/10.1021/acsomega.3c06775
ACS Omega 2023, 8, 46955−46966

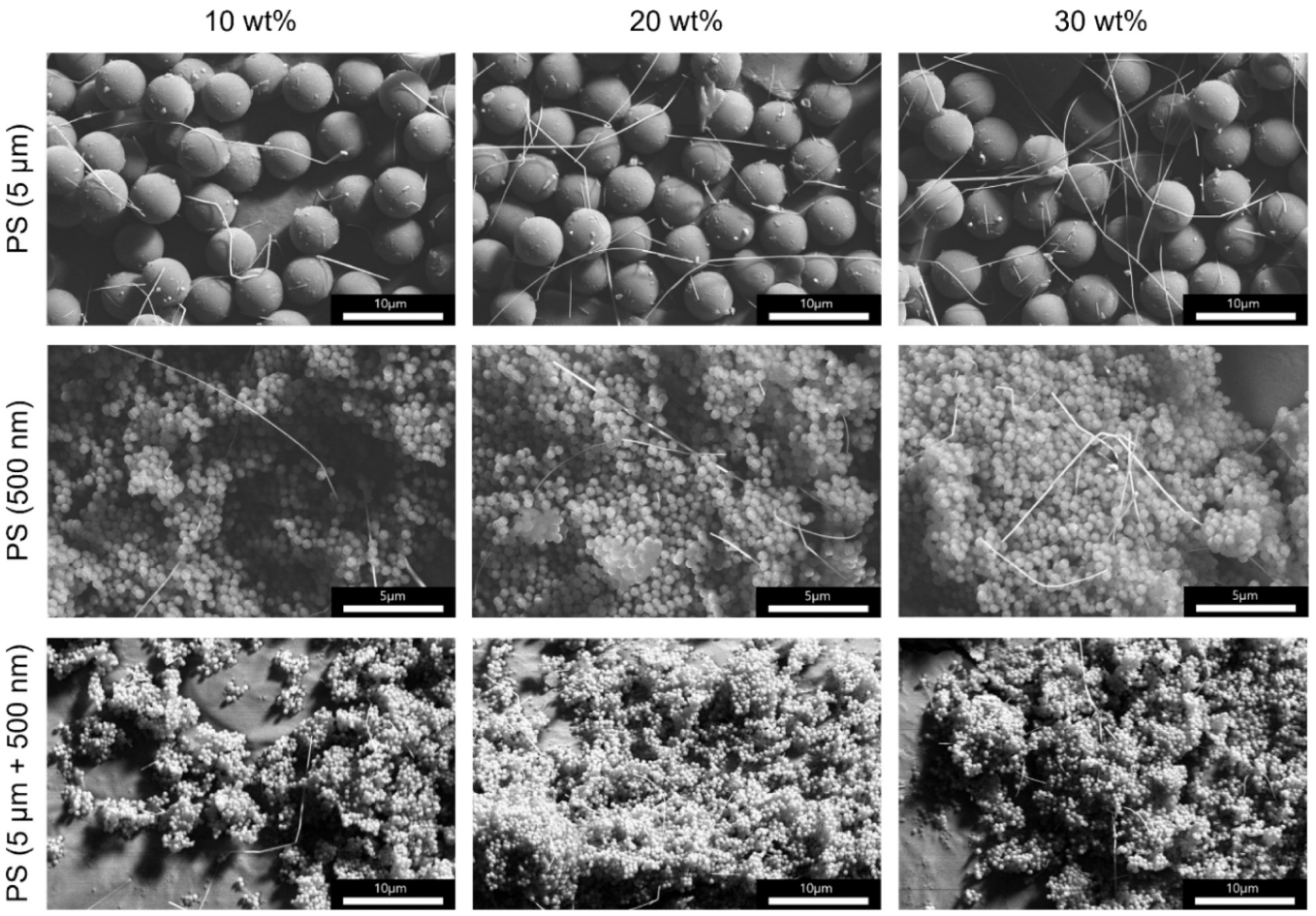

Figure 7. SEM images of CuNW/PS mixtures with different PS particle sizes and CuNW contents before the compounding process.

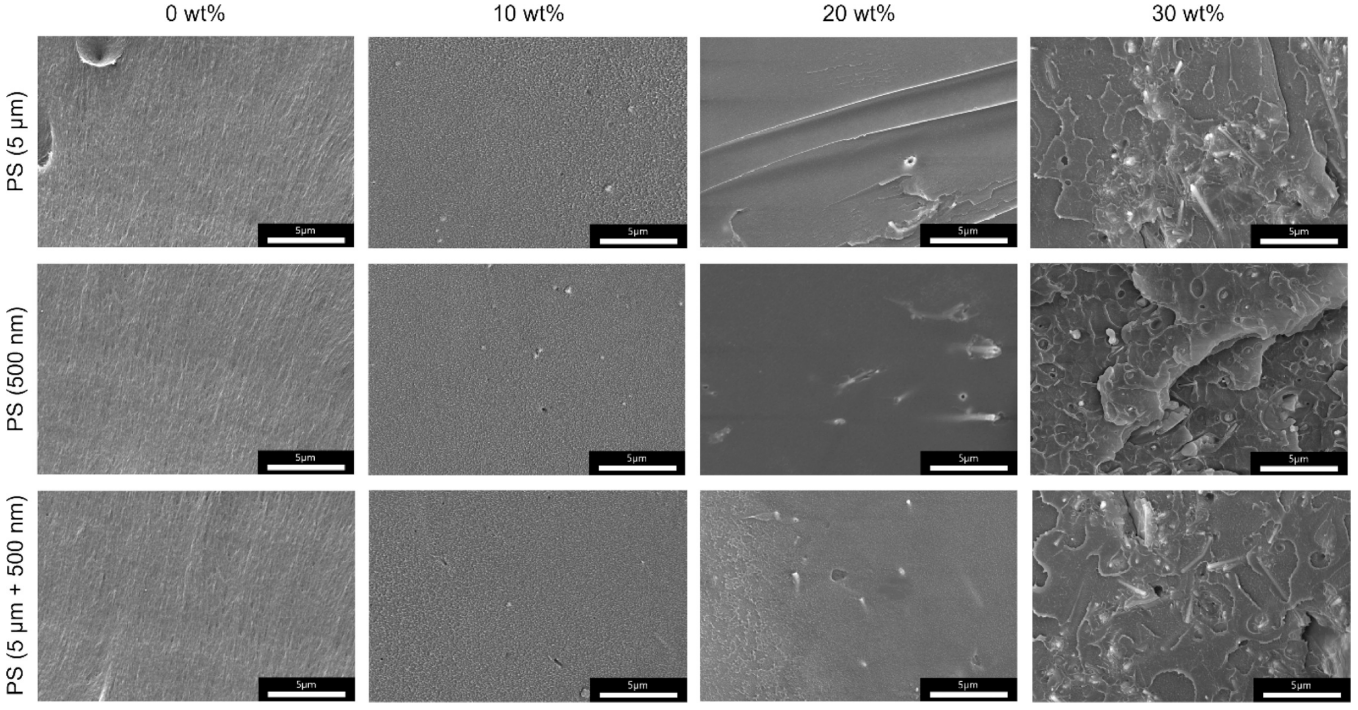

Figure 8. SEM images of fractured surfaces of PS/CuNW nanocomposites with different PS particle sizes and CuNW loadings after the compounding process (thermal compression).

https://doi.org/10.1021/acsomega.3c06775
ACS Omega 2023, 8, 46955−46966

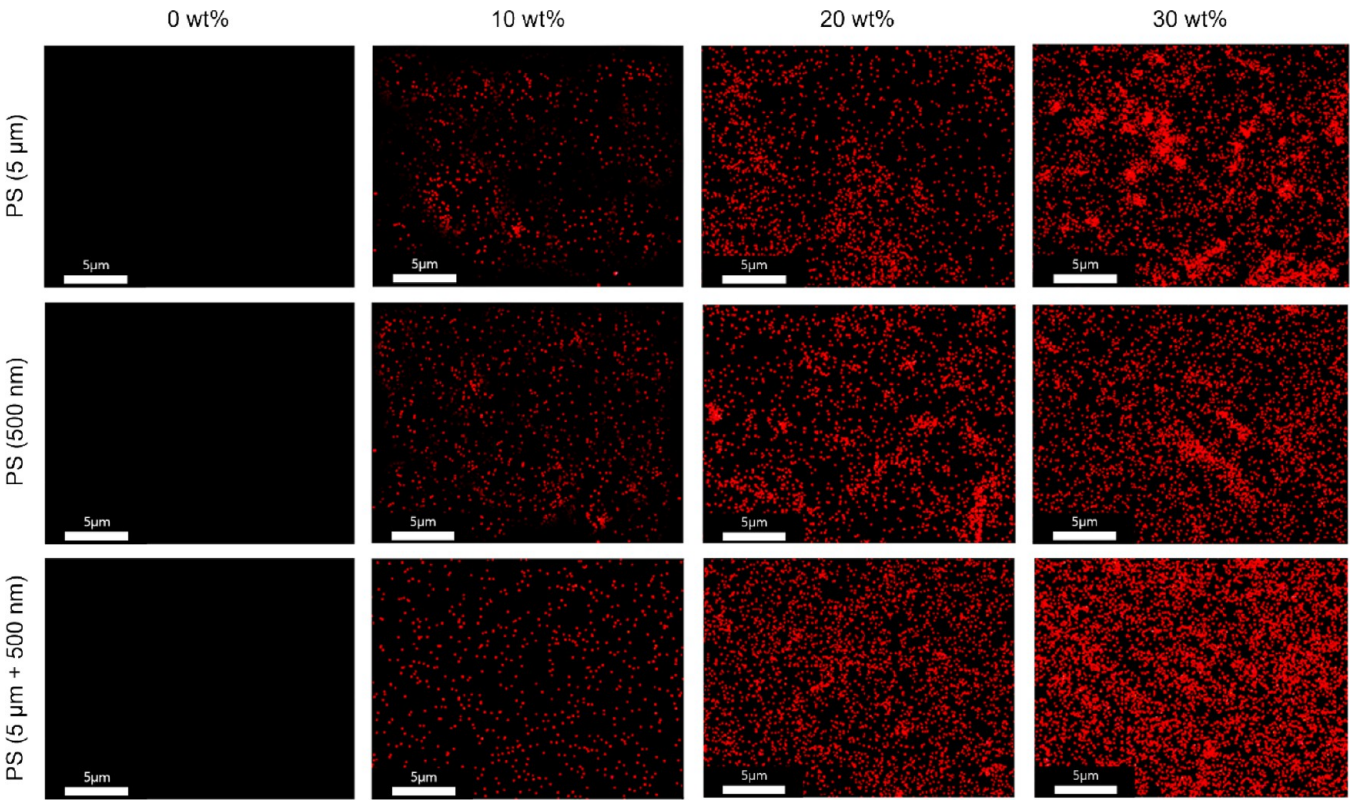

Figure 9. Cu mapping (FE-SEM/EDX) images of CuNW/PS nanocomposites with different PS particle sizes and CuNW contents.

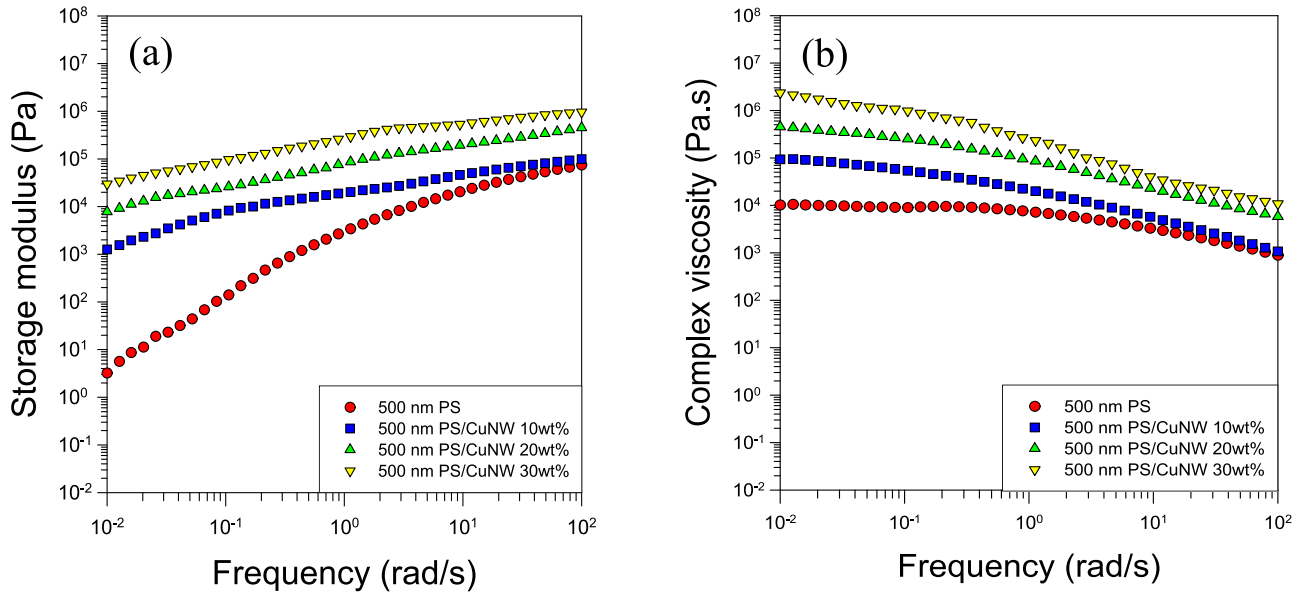

Figure 10. Rheological properties of CuNW/PS (500 nm diameter) nanocomposites: (a) storage modulus and (b) complex viscosity.

of Cu in Figure 9. The CuNWs were homogeneously dispersed within the PS polymer matrix regardless of the PS particle size and CuNW loading. This indicates that uniform dispersion was achieved without the aid of other dispersants, relying solely on mechanical and ultrasonic dispersions with IPA.

3.4. Rheological Properties of CuNW/PS Nanocomposites. The dispersion of conductive nanofillers within a polymer matrix and the viscoelastic characteristics of nanocomposites in a dynamic condition can be analyzed by evaluating the rheological properties, such as the storage modulus (G'), loss modulus (G''), and complex viscosity (η^*). Figure 10 presents the G' and η^* values of CuNW/PS (500 nm) nanocomposites with different CuNW concentrations in the frequency range from 0.01 to 100 rad/s. As shown in Figure 10a, G' had smaller increments in the high-frequency region than in the low-frequency region. This is because the influence of the nanofillers was significant in the low-frequency region whereas the physical network structure of CuNWs was disrupted in the high-frequency region, and thus the polymer matrix dominated the overall characteristics of the nano-

https://doi.org/10.1021/acsomega.3c06775
ACS Omega 2023, 8, 46955−46966

composites rather than the CuNW. In addition, a more robust network of CuNWs was formed within the PS matrix with increasing CuNW content, leading to solid-like characteristics and a decreasing slope of G'. Figure 10b shows that the η^* values of all CuNW/PS (500 nm) nanocomposite samples decreased as a function of frequency, which is a typical behavior of polymer melts. When CuNWs were embedded in the PS, the η^* of the nanocomposites exhibited a sharp change in the low-frequency region, indicating restriction of the flow behavior due to the CuNW network formation. Furthermore, it is rheologically well known that as the G''/G' (tan δ) value approaches 0, the behavior is dominated by elasticity, while as it approaches infinity, the behavior is dominated by viscosity. The tan δ value approached 0 with an increase in the CuNW concentration, as summarized in Table 2, indicating that G' was higher than the G'' because of elastic-dominant behavior.

Table 2. Storage Modulus, Loss Modulus, and Tan δ of PS/CuNW Nanocomposites with Different CuNW Contents Evaluated at 1 rad/s

CuNW content (wt %)	G' (Pa)	G'' (Pa)	tan δ
0	3420	7340	2.15
10	20,200	15,700	0.78
20	86,900	41,100	0.47
30	294,000	73,200	0.25

3.5. Electrical Properties of CuNW/PS Nanocomposites. The electrical conductivity of polymer nanocomposites significantly depends on the content of the conductive nanofillers. The incorporation of conductive nanofillers into an insulating polymer matrix brings about a conductive network within the insulating polymer matrix at a specific concentration, thereby substantially increasing the electrical conductivity. This concentration is known as the percolation threshold.[46] The percolation threshold can be determined using the power−law relationship (eq 3).

$$\sigma \propto (m - m_c)^b \tag{3}$$

where σ, m, m_c, and b represent the electrical conductivity of CuNWs, weight percent of CuNWs, electrical percolation threshold, and critical exponent related to the system dimension, respectively.[47] For 1D fiber-embedded systems of polymer nanocomposites, the b value typically has a value close to or greater than 2.[45] In this study, the b values of nanocomposites were 1.9, 1.7, and 1.6 for nanocomposites containing 5 μm PS microspheres, 500 nm PS microspheres, and mixed (5 and 500 nm) PS particles, respectively. All b values were close to 2, thereby indicating that the CuNWs in the nanocomposites were dispersed similar to 1D fiber systems. The electrical conductivity of nanocomposites increased with an increase in the CuNW content from 10^{-11}−10^{-10} to ca. 10° S/m for 0 to 30 wt %, respectively, regardless of the PS particles, as shown in Figure 11a. The electrical conductivity of the nanocomposite containing 500 nm PS microspheres was higher than that of 5 μm PS microspheres. This is because the smaller PS particles allowed for more uniform dispersion of CuNWs in the PS matrix owing to the smaller amount of steric hindrance, thereby minimizing CuNW aggregation. In particular, the nanocomposite comprising different sizes (500 nm and 5 μm) of PS spheric particles exhibited the highest electrical conductivity among the three samples. This was attributed to the 500 nm PS microspheres filling the voids

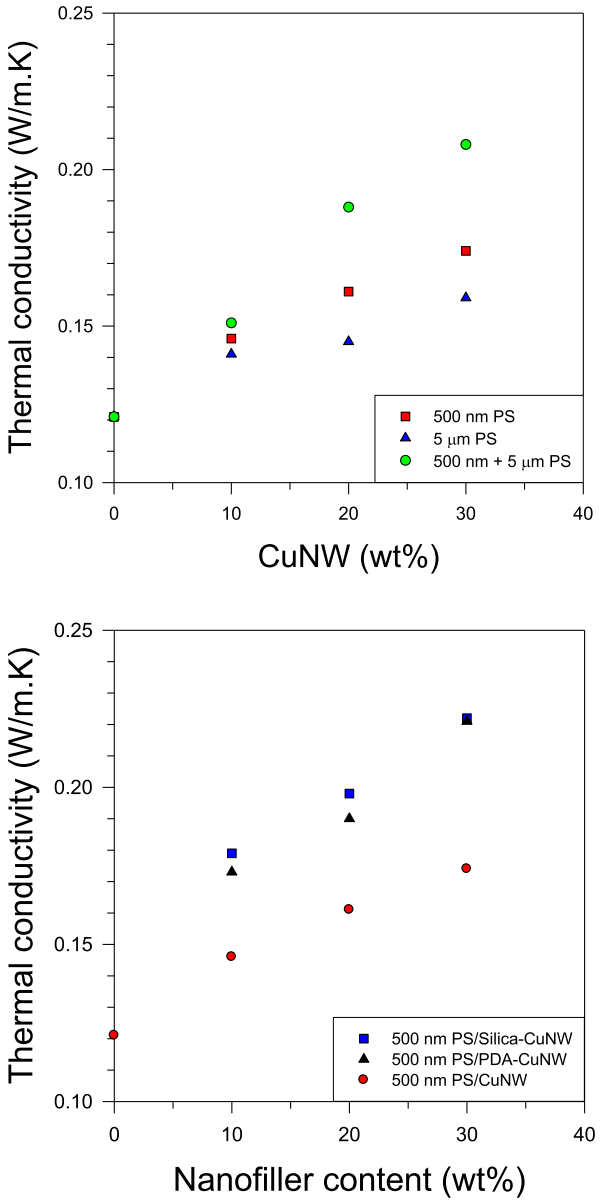

Figure 11. Electrical conductivities of nanocomposites: (a) CuNW/PS with different PS particle sizes and CuNW contents and (b) CuNW/PS (500 nm) nanocomposites with and without surface-modified CuNWs.

between the 5 μm PS microspheres, minimizing the amount of space for CuNW conductive nanofiller aggregation and achieving more uniform dispersion. Uniform dispersion enabled the formation of a more robust conductive network structure within the polymer matrix, ultimately enhancing the electrical conductivity of the composite. The percolation threshold (m_c) appeared to be approximately 5 wt % for all cases, based on the power−law equation. The m_c typically decreased with increasing aspect ratio or dispersion of the nanofiller owing to the formation of a more robust conductive network structure.[48] The different sizes of the matrix particles at identical nanofiller concentrations slightly influenced the electrical conductivity, whereas the different contents of nanofillers at identical PS size led to a significant difference in electrical conductivity.

Within the domain of electrical applications, the consensus regarding the advantages of possessing reliable thermal and

https://doi.org/10.1021/acsomega.3c06775
ACS Omega 2023, 8, 46955−46966

electrically conductive qualities is well-established. Nevertheless, instances arise where the usefulness pertains to materials that offer both electrical insulation and efficient heat conduction. Therefore, in addition to CuNW/PS, SiO_2- and PDA-coated CuNW/PS (500 nm in diameter) nanocomposites exhibiting thermal conduction and electrical insulation were examined for TIM applications. As shown in Figure 11b, the electrical insulations of both SiO_2−CuNW/PS and PDA-CuNW/PS were maintained with the incorporation of up to 30 wt % nanofiller. The incorporation of modified CuNWs into the polymer matrix exhibited a reduction in the electrical conductivity attributed to the presence of an insulating coating. Specifically, when subjected to 30 wt %, the electrical conductivity underwent a pronounced decrease, transitioning from 10^{0} S/m to the range of 10^{-8} to 10^{-10} S/m, thus rendering the nanowires insulating in nature. In the case of PDA-CuNWs, the electrical conductivity was higher than that of SiO_2−CuNWs because the PDA insulation coating was partially removed. The PDA layer coated on CuNW became detached and broken owing to its lower robustness, compared to the inorganic SiO_2, which is ascribed to the SEM results, as shown in Figure 5c. The CuNW surfaces stripped of the PDA coating layer were in contact with each other, thereby producing an unwanted electrically conductive network.

3.6. Thermal Properties of CuNW/PS Nanocomposites. Electrical conductivity is commonly accompanied by thermal conductivity. Thus, the thermal conductivities of CuNW/PS nanocomposites with different PS particle sizes and CuNW concentrations were measured. The thermal conductivity of the CuNW-incorporated PS nanocomposites exceeded that of pristine PS without CuNW, regardless of the size of the PS particles, as shown in Figure 12a. The thermal conductivities of the nanocomposites of both monodisperse and mixed PS particles increased with increasing CuNW loading. The nanocomposites containing 500 nm PS microspheres as the matrix exhibited higher thermal conductivities than those composed of 5 μm PS spheric particles. This was attributed to the empty spaces between the PS particles and the dispersion of CuNW within the PS polymer matrix. Relatively larger empty spaces in the case of 5 μm PS particles allowed for the formation of agglomerated nanofillers, indicating poorer dispersion compared to the case of 500 nm PS microspheres where a more efficient thermal transfer network structure with better dispersion of CuNW was formed. The nanocomposites containing mixed PS particles with diameters of 500 nm and 5 μm exhibited the highest thermal conductivity. In this case, 500 nm PS particles filled the voids among 5 μm PS particles, resulting in a denser CuNW/PS nanocomposite.

Electrical insulation was achieved by coating CuNWs with inorganic and organic substances. The thermal conductivities of the surface-modified CuNW/PS nanocomposites increased as a function of nanofiller content (Figure 12b). For instance, the thermal conductivity of 500 nm PS composites containing SiO_2−CuNW increased from 0.12 to 0.18 W/m·K for 0 to 10 wt % of nanofiller, respectively. This indicates that the surface-modified CuNW/PS nanocomposites showed thermal conductivity superior to the unmodified CuNW/PS nanocomposites. The thermal conductivities of the SiO_2−CuNW/PS nanocomposites were slightly higher than those of the PDA-CuNW/PS nanocomposites because the tendency of PDA-CuNW to aggregate in the PS matrix is generally greater than that of SiO_2−CuNW, thereby reducing the PDA-CuNW dispersion within the PS matrix.[49] In contrast to the electrical properties of the nanocomposites, the surface-modified CuNW/PS nanocomposites exhibited higher thermal conductivities than the unmodified CuNW/PS nanocomposites because the surface coating improved the dispersion of nanofillers within the PS/IPA solution during the mixing process, ultimately yielding more uniform dispersion in the PS matrix caused by superior dispersion in water during preparation. For instance, the thermal conductivity of 500 nm PS composites containing surface-modified CuNW of 30 wt % increased from 0.12 to 0.22 W/m·K.

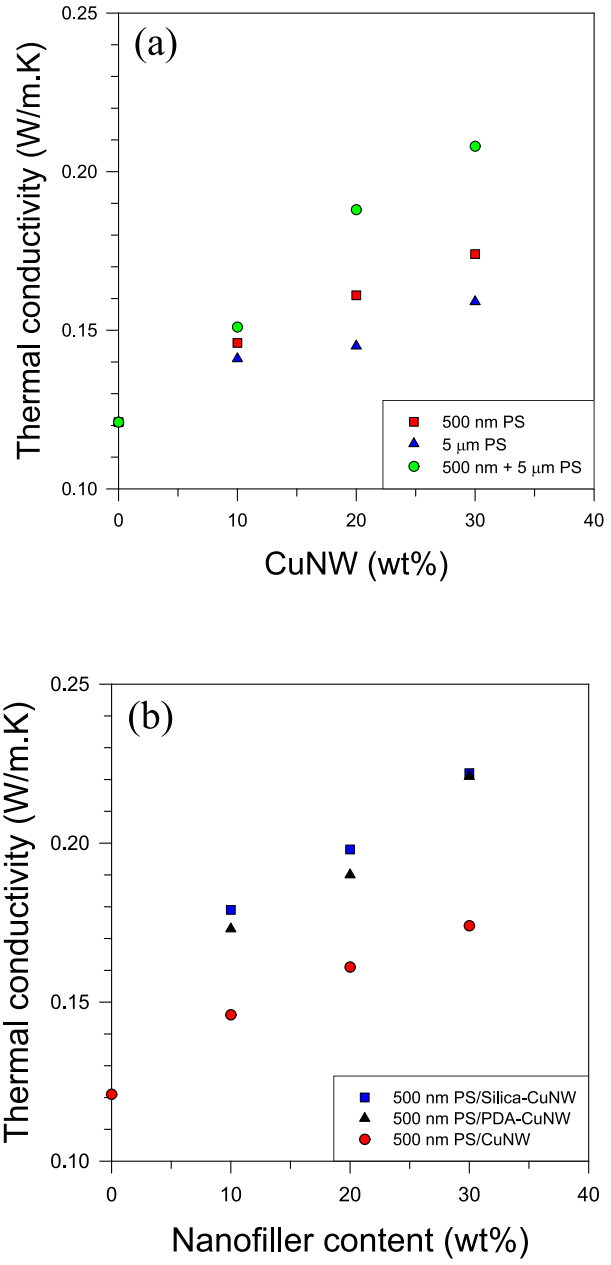

Figure 12. Thermal conductivities of nanocomposites: (a) CuNW/PS nanocomposites with different PS particle sizes and CuNW contents and (b) surface-modified CuNW/PS (500 nm in diameter) nanocomposites.

https://doi.org/10.1021/acsomega.3c06775
ACS Omega 2023, 8, 46955−46966

4. CONCLUSIONS

In this study, monodisperse PS microspheres with sizes of 5 μm and 500 nm were synthesized as polymer matrices via dispersion and emulsifier-free emulsion polymerization, respectively. CuNWs with average diameters, lengths, and aspect ratios of approximately 100 nm, 55 μm, and 550, respectively, were synthesized as conductive nanofillers using an aqueous media reduction. Using the monodisperse and bidisperse (5 μm and 500 nm) PS particles and CuNWs, conductive polymer nanocomposites (CuNW/PS) were manufactured. The surfaces of CuNWs were coated with SiO_2 and PDA to confer electrical insulation and maintain the thermal conductivity for TIM applications. The morphological, rheological, electrical, and thermal properties of the CuNW/PS nanocomposites were analyzed. The nanofillers were uniformly dispersed within the polymer matrix, regardless of the PS particle size and CuNW content. The CuNW/PS nanocomposites exhibited elastic-dominant behavior, with G' exceeding G'' at all frequencies, which indicated tan δ close to 0. The electrical and thermal conductivities of nanocomposites increased with increasing CuNW. Among the samples tested, the nanocomposite with mixed PS particles had the highest electrical conductivity (from 1×10^{-11} to 1×10^{0} S/m). When silica- and PDA-coated CuNWs were used as nanofillers, insulation properties (10^{-10}–10^{-9} S/m) were achieved while increasing thermal conductivity (approximately 0.17 to 0.22 W/m·K for the composite containing 500 nm PS and 30 wt % CuNW), which is advantageous for TIM applications. In summary, this work stands out in the field of nanocomposites by combining multiple approaches, such as the use of mixed particle sizes and surface modification of CuNW for electrical insulation with good thermal conductivity. The combination of these multifaceted strategies in this study generated superior properties, notably remarkable enhancements in electrical insulation and thermal properties, although each aspect has previously been examined individually. These contributions pave the way for the development of advanced materials for electrical and thermal management.

AUTHOR INFORMATION

Corresponding Authors

Keon-Soo Jang − *Department of Polymer Engineering, The University of Suwon, Hwaseong, Gyeonggi 18323, South Korea*; orcid.org/0000-0002-0883-2683; Email: ksjang@suwon.ac.kr

Seong Jae Lee − *Department of Polymer Engineering, The University of Suwon, Hwaseong, Gyeonggi 18323, South Korea*; orcid.org/0000-0001-5514-3234; Email: sjlee@suwon.ac.kr

Authors

Hyeon Sik Eom − *Department of Polymer Engineering, The University of Suwon, Hwaseong, Gyeonggi 18323, South Korea*

Dong Won Kim − *Department of Polymer Engineering, The University of Suwon, Hwaseong, Gyeonggi 18323, South Korea*

Complete contact information is available at: https://pubs.acs.org/10.1021/acsomega.3c06775

Notes

The authors declare no competing financial interest.

ACKNOWLEDGMENTS

The authors gratefully acknowledge the National Research Foundation of Korea (NRF), funded by the Korean government (MSIT) (NRF-2018R1A5A1024127 and NRF-2021R1F1A1063116).

REFERENCES

(1) Jordan, J.; Jacob, K. I.; Tannenbaum, R.; Sharaf, M. A.; Jasiuk, I. Experimental Trends in Polymer Nanocomposites—a Review. *Mater. Sci. Eng., A* **2005**, *393* (1), 1−11.

(2) Singh, A.; Prabhu, T. R.; Sanjay, A. R.; Koti, V. An Overview of Processing and Properties of CU/CNT Nano Composites. *Mater. Today: Proc.* **2017**, *4* (2,Part A), 3872−3881.

(3) Shen, S.; Yang, L.; Wang, C.; Wei, L. Effect of CNT Orientation on the Mechanical Property and Fracture Mechanism of Vertically Aligned Carbon Nanotube/Carbon Composites. *Ceram. Int.* **2020**, *46* (4), 4933−4938.

(4) Sofiah, A. G. N.; Samykano, M.; Kadirgama, K.; Mohan, R. V.; Lah, N. A. C. Metallic nanowires: Mechanical Properties − Theory and Experiment. *Appl. Mater. Today* **2018**, *11*, 320−337.

(5) Castro Neto, A. H.; Guinea, F.; Peres, N. M. R.; Novoselov, K. S.; Geim, A. K. The Electronic Properties of Graphene. *Rev. Mod. Phys.* **2009**, *81* (1), 109−162.

(6) Pascual, J. I.; Méndez, J.; Gómez-Herrero, J.; Baró, A. M.; Garcia, N.; Landman, U.; Luedtke, W. D.; Bogachek, E. N.; Cheng, H.-P. Properties of Metallic nanowires: From Conductance Quantization to Localization. *Science* **1995**, *267* (5205), 1793−1795.

(7) Ciprari, D.; Jacob, K.; Tannenbaum, R. Characterization of Polymer Nanocomposite Interphase and Its Impact on Mechanical Properties. *Macromolecules* **2006**, *39* (19), 6565−6573.

(8) Fu, S.; Sun, Z.; Huang, P.; Li, Y.; Hu, N. Some Basic Aspects of Polymer Nanocomposites: A Critical Review. *Nano Mater. Sci.* **2019**, *1* (1), 2−30.

(9) Gam, S.; Meth, J. S.; Zane, S. G.; Chi, C.; Wood, B. A.; Winey, K. I.; Clarke, N.; Composto, R. J. Polymer Diffusion in a Polymer Nanocomposite: Effect of Nanoparticle Size and Polydispersity. *Soft Matter* **2012**, *8* (24), 6512−6520.

(10) Grossiord, N.; Loos, J.; van Laake, L.; Maugey, M.; Zakri, C.; Koning, C. E.; Hart, A. J. High-Conductivity Polymer Nanocomposites Obtained by Tailoring the Characteristics of Carbon Nanotube Fillers. *Adv. Funct. Mater.* **2008**, *18* (20), 3226−3234.

(11) Sureshkumar, M.; Na, H. Y.; Ahn, K. H.; Lee, S. J. Conductive Nanocomposites Based on Polystyrene Microspheres and Silver nanowires by Latex Blending. *ACS Appl. Mater. Interfaces* **2015**, *7* (1), 756−764.

(12) Brooks, B. Suspension Polymerization Processes. *Chem. Eng. Technol.* **2010**, *33* (11), 1737−1744.

(13) Erbay, E.; Bilgiç, T.; Karali, M.; Savaşçi, Ö. T. Polystyrene Suspension Polymerization: The Effect of Polymerization Parameters on Particle Size and Distribution. *Polym.-Plast. Technol. Eng.* **1992**, *31* (7−8), 589−605.

(14) Lu, Y. Y.; El-Aasser, M. S.; Vanderhoff, J. W. Dispersion Polymerization of Styrene in Ethanol: Monomer Partitioning Behavior and Locus of Polymerization. *J. Polym. Sci., Part B: Polym. Phys.* **1988**, *26* (6), 1187−1203.

(15) Sáenz, J. M.; Asua, J. M. Dispersion Polymerization in Polar Solvents. *J. Polym. Sci. Part Polym. Chem.* **1995**, *33* (9), 1511−1521.

(16) Song, J.-S.; Winnik, M. A. Cross-Linked, Monodisperse, Micron-Sized Polystyrene Particles by Two-Stage Dispersion Polymerization. *Macromolecules* **2005**, *38* (20), 8300−8307.

(17) Chaitidou, S.; Kotrotsiou, O.; Kotti, K.; Kammona, O.; Bukhari, M.; Kiparissides, C. Precipitation Polymerization for the Synthesis of Nanostructured Particles. *Mater. Sci. Eng., B* **2008**, *152* (1), 55−59.

(18) Thickett, S. C.; Gilbert, R. G. Emulsion Polymerization: State of the Art in Kinetics and Mechanisms. *Polymer* **2007**, *48* (24), 6965−6991.

(19) Schork, F. J.; Luo, Y.; Smulders, W.; Russum, J. P.; Butté, A.; Fontenot, K. Miniemulsion Polymerization. In *Polymer Particles*;

https://doi.org/10.1021/acsomega.3c06775
ACS Omega 2023, 8, 46955−46966

Advances in Polymer Science; Springer: Berlin, Heidelberg, 2005; pp 129−255. DOI: 10.1007/b100115.
(20) Tuncel, A.; Kahraman, R.; Pişkin, E. Monosize Polystyrene Microbeads by Dispersion Polymerization. *J. Appl. Polym. Sci.* **1993**, *50* (2), 303−319.
(21) Shim, S. E.; Yang, S.; Choi, H. H.; Choe, S. Fully Crosslinked Poly(Styrene-Co-Divinylbenzene) Microspheres by Precipitation Polymerization and Their Superior Thermal Properties. *J. Polym. Sci. Part Polym. Chem.* **2004**, *42* (4), 835−845.
(22) Sharifi-Sanjani, N.; Soltan-Dehghan, M.; Naderi, N.; Ranji, A. Emulsifier-Free Emulsion Polymerization of Styrene. *J. Appl. Polym. Sci.* **2004**, *94* (5), 1898−1904.
(23) Song, Z.; Poehlein, G. W. Kinetics of Emulsifier-Free Emulsion Polymerization of Styrene. *J. Polym. Sci. Part Polym. Chem.* **1990**, *28* (9), 2359−2392.
(24) Cheng, Y.; Wang, S.; Wang, R.; Sun, J.; Gao, L. Copper Nanowire Based Transparent Conductive Films with High Stability and Superior Stretchability. *J. Mater. Chem. C* **2014**, *2* (27), 5309−5316.
(25) Wade, T. L.; Wegrowe, J.-E. Template Synthesis of Nanomaterials. *Eur. Phys. J. - Appl. Phys.* **2005**, *29* (1), 3−22.
(26) Liu, Y.; Goebl, J.; Yin, Y. Templated Synthesis of Nanostructured Materials. *Chem. Soc. Rev.* **2013**, *42* (7), 2610−2653.
(27) El-Giar, E. M.; Said, R. A.; Bridges, G. E.; Thomson, D. J. Localized Electrochemical Deposition of Copper Microstructures. *J. Electrochem. Soc.* **2000**, *147* (2), 586.
(28) Zhang, D.; Wang, R.; Wen, M.; Weng, D.; Cui, X.; Sun, J.; Li, H.; Lu, Y. Synthesis of Ultralong Copper nanowires for High-Performance Transparent Electrodes. *J. Am. Chem. Soc.* **2012**, *134* (35), 14283−14286.
(29) Mock, J.; Bobinger, M.; Bogner, C.; Lugli, P.; Becherer, M. Aqueous Synthesis, Degradation, and Encapsulation of Copper nanowires for Transparent Electrodes. *Nanomaterials* **2018**, *8* (10), 767.
(30) Mohl, M.; Pusztai, P.; Kukovecz, A.; Konya, Z.; Kukkola, J.; Kordas, K.; Vajtai, R.; Ajayan, P. M. Low-Temperature Large-Scale Synthesis and Electrical Testing of Ultralong Copper nanowires. *Langmuir* **2010**, *26* (21), 16496−16502.
(31) Rathmell, A. R.; Wiley, B. J. The Synthesis and Coating of Long, Thin Copper nanowires to Make Flexible, Transparent Conducting Films on Plastic Substrates. *Adv. Mater.* **2011**, *23* (41), 4798−4803.
(32) Jin, M.; He, G.; Zhang, H.; Zeng, J.; Xie, Z.; Xia, Y. Shape-Controlled Synthesis of Copper Nanocrystals in an Aqueous Solution with Glucose as a Reducing Agent and Hexadecylamine as a Capping Agent. *Angew. Chem., Int. Ed.* **2011**, *50* (45), 10560−10564.
(33) Coetzee, D.; Venkataraman, M.; Militky, J.; Petru, M. Influence of Nanoparticles on Thermal and Electrical Conductivity of Composites. *Polymers* **2020**, *12* (4), 742.
(34) Schwamb, T.; Burg, B. R.; Schirmer, N. C.; Poulikakos, D. An Electrical Method for the Measurement of the Thermal and Electrical Conductivity of Reduced Graphene Oxide Nanostructures. *Nanotechnology* **2009**, *20* (40), No. 405704.
(35) Moisala, A.; Li, Q.; Kinloch, I. A.; Windle, A. H. Thermal and Electrical Conductivity of Single- and Multi-Walled Carbon Nanotube-Epoxy Composites. *Compos. Sci. Technol.* **2006**, *66* (10), 1285−1288.
(36) Wang, X.; Wu, P. Highly Thermally Conductive Fluorinated Graphene Films with Superior Electrical Insulation and Mechanical Flexibility. *ACS Appl. Mater. Interfaces* **2019**, *11* (24), 21946−21954.
(37) Niu, H.; Ren, Y.; Guo, H.; Małycha, K.; Orzechowski, K.; Bai, S.-L. Recent Progress on Thermally Conductive and Electrical Insulating Rubber Composites: Design. *Processing and Applications. Compos. Commun.* **2020**, *22*, No. 100430.
(38) Moore, A. L.; Shi, L. Emerging Challenges and Materials for Thermal Management of Electronics. *Mater. Today* **2014**, *17* (4), 163−174.
(39) Wan, L.; Feng, J.; Yue, W.; Qin, W.; Lin, F.; Huang, F.; Liu, X.; Min, X.; Wang, C.; Huang, Z. Skin-Inspired Thermosensitive Tactile Sensor Based on Thermally Conductive and Viscous Interface Composites for Rocks. *Adv. Eng. Mater.* **2023**, *25* (19), No. 2300469.
(40) Hu, X.; Huang, M.; Kong, N.; Han, F.; Tan, R.; Huang, Q. Enhancing the Electrical Insulation of Highly Thermally Conductive Carbon Fiber Powders by SiC Ceramic Coating for Efficient Thermal Interface Materials. *Compos. Part B Eng.* **2021**, *227*, No. 109398.
(41) Razeeb, K. M.; Dalton, E.; Cross, G. L. W.; Robinson, A. J. Present and Future Thermal Interface Materials for Electronic Devices. *Int. Mater. Rev.* **2018**, *63* (1), 1−21.
(42) Ma, H.; Gao, B.; Wang, M.; Yuan, Z.; Shen, J.; Zhao, J.; Feng, Y. Strategies for Enhancing Thermal Conductivity of Polymer-Based Thermal Interface Materials: A Review. *J. Mater. Sci.* **2021**, *56* (2), 1064−1086.
(43) Prasher, R. Thermal Interface Materials: Historical Perspective, Status, and Future Directions. *Proc. IEEE* **2006**, *94* (8), 1571−1586.
(44) Kim, K.; Ahn, K.; Ju, H.; Kim, J. Improvement of Insulating and Thermal Properties of SiO2-Coated Copper Nanowire Composites. *Ind. Eng. Chem. Res.* **2016**, *55* (10), 2713−2720.
(45) Yuan, H.; Wang, Y.; Li, T.; Ma, P.; Zhang, S.; Du, M.; Chen, M.; Dong, W.; Ming, W. Highly Thermal Conductive and Electrically Insulating Polymer Composites Based on Polydopamine-Coated Copper Nanowire. *Compos. Sci. Technol.* **2018**, *164*, 153−159.
(46) Du, F.; Fischer, J. E.; Winey, K. I. Effect of Nanotube Alignment on Percolation Conductivity in Carbon Nanotube/Polymer Composites. *Phys. Rev. B* **2005**, *72* (12), No. 121404.
(47) Hu, G.; Zhao, C.; Zhang, S.; Yang, M.; Wang, Z. Low Percolation Thresholds of Electrical Conductivity and Rheology in Poly(Ethylene Terephthalate) through the Networks of Multi-Walled Carbon Nanotubes. *Polymer* **2006**, *47* (1), 480−488.
(48) Celzard, A.; McRae, E.; Deleuze, C.; Dufort, M.; Furdin, G.; Marêché, J. F. Critical Concentration in Percolating Systems Containing a High-Aspect-Ratio Filler. *Phys. Rev. B* **1996**, *53* (10), 6209−6214.
(49) Nguyen, H. A.; Lee, N. Y. Polydopamine Aggregation: A Novel Strategy for Power-Free Readout of Loop-Mediated Isothermal Amplification Integrated into a Paper Device for Multiplex Pathogens Detection. *Biosens. Bioelectron.* **2021**, *189*, No. 113353.

NOTE ADDED AFTER ASAP PUBLICATION

This paper originally published ASAP on November 29, 2023. Due a production error, panel C in Figure 4 was incorrect. A new version reposted on November 30, 2023.

https://doi.org/10.1021/acsomega.3c06775
ACS Omega 2023, 8, 46955−46966